**ISSN: 0067-2904**

# Non-Resonant Reaction Rates of $^{13}C(\alpha,n)^{16}O$ and $^{22}Ne(\alpha,n)^{25}Mg$ reactions in AGB Stars

**Lana T. Ali*, Ahmed A. Selman**
Department of Astronomy and Space, College of Science, University of Baghdad, Baghdad-Iraq

Received: 14/7/2020 Accepted: 9/10/2020

**Abstract**

Both $^{13}C(\alpha,n)^{16}O$ and $^{22}Ne(\alpha,n)^{25}Mg$ reactions perform a cosmic role in the production of neutrons in AGB stars, which significantly contributes to the nucleosynthesis via the *s-process*. The astrophysical S-factor for both reactions is calculated in this research, utilizing EMPIRE code and depending on two parameter sets for the optical potential. These datasets were published earlier by McFadden and Satchler (denoted here as MFS) and Avrigeanu and Hodgson (denoted as AH) for the non-resonant region of the spectrum and over a temperature range of $0.01-1$ GK. The extrapolated S-factor at zero energy is derived to be $1.48\times10^{6}$ MeV and $3.7\times10^{6}$ MeV for $^{13}C(\alpha,n)^{16}O$, while the values were $1.0\times10^{9}$ MeV and $2.6\times10^{9}$ MeV for $^{22}Ne(\alpha,n)^{25}Mg$, using MFS and AH parameter sets, respectively, which showed a reasonable agreement with the most recommended value. The differences in the S-factor, $S(E)$, values obtained from these two adopted parameter sets are attributed to the variations of the real potential term's diffuseness parameter that affects the reaction cross section, hence S-factor, specifically at low energy region. Moreover, the present results imply an influential enhancement of the rates by the electron shielding effect at the low-temperature region $T<0.1$GK, in which $^{13}C(\alpha,n)^{16}O$ reaction is activated, especially on $^{22}Ne(\alpha,n)^{25}Mg$ reaction. In addition, for both adopted reactions and overall selected temperature range, the reaction rates using $S(E)$ values based on MFS showed acceptable results compared with previous compilations and reference libraries. While the results obtained from AH exceeded all the other compilations even though the resonance contributions are currently unconsidered.

**Keywords**: nuclear reaction, S-factor, screening effect, and AGB stars.

# معدلات التفاعل الغير الرنيني لتفاعلات $^{13}C(\alpha,n)^{16}O$ و $^{22}Ne(\alpha,n)^{25}Mg$ في نجوم AGB

**لانه طالب علي *، احمد عبد الرزاق سلمان**
قسم الفلك والفضاء, كلية العلوم, جامعة بغداد, العراق

**الخلاصة**

يؤدي كل من التفاعلين $^{13}C(\alpha,n)^{16}O$ و $^{22}Ne(\alpha,n)^{25}Mg$ دوراً كونياً اساسياً في توليد النيوترونات في نجوم AGB والتي بدورها تساهم بصورة كبيرة في عملية أنتاج النوى من خلال عملية الاقتناص النيوتروني البطيء s–process. تم حساب المعامل الفلكي S–factor لكلا التفاعلين المختارين في هذا البحث باستخدام برنامج EMPIRE, وبالاعتماد على مجموعتين من المعاملات الفيزيائية للجهد البصري وهما معاملات مكفيدن وساتشلر MFS ومعاملات افيرجينو و هودجسون AH للمنطقة الغير الرنانه من الطيف,

*Email: lana.t.ali@scbaghdad.edu.iq

و على مدى درجات حرارة بين 0.01 الى 1 غيغا كلفن. وقد تم الاستنتاج بأن قيمة المعامل الفلكي عند الطاقة الصفرية بأنها تساوي $1.48 \times 10^6$ ميكا الكترون فولط و $3.7 \times 10^6$ ميكا الكترون فولط لتفاعل $^{13}C(\alpha,n)^{16}O$ $1.0 \times 10^9$ ميكا الكترون فولط و $2.6 \times 10^9$ ميكا الكترون فولط لتفاعل $^{22}Ne(\alpha,n)^{25}Mg$ من أستخدام مجموعتي معاملات MFS و AH على الترتيب، و أظهرت تطابق جيد مع أكثر القيم المعتمدة. لقد عزيت الفروق في قيم المعامل الفلكي S−factor, S(E), الى الاختلاف في معامل الانتشار الخاص بالقيم الحقيقية للجهد البصري والتي تؤثر على قيمة مساحة التفاعل وبالتالي المعامل الفلكي S−factor و خصوصا في مدى الطاقات الواطئة. علاوة على ذلك اشرت النتائج الحالية الى وجود زيادة مؤثرة في قيم معدلات التفاعل بسبب تأثير حجب الجهد الالكتروني في مدى الطاقات الواطيء (أقل من 0.01) والتي يتم عندها تنشيط تفاعل $^{13}C(\alpha,n)^{16}O$, وخاصةً في حساب معدلات تفاعل $^{22}Ne(\alpha,n)^{25}Mg$.بالأضافة الى ذلك, أظهرت قيم معدلات التفاعل الناتجة من استخدام $S(E)$ الناتج من معاملات MFS, نتائج مقبولة لكلا التفاعلين المختارين في هذا البحث وعلى مدى جميع درجات الحرارة المحددة, مقارنة مع النتائج السابقة للمجموعات والمكتبات المرجعية. في حين أن تلك التي تم الحصول عليها من AH تتجاوز جميع القيم المنشوره سابقاً على الرغم من أن المعالجة الحالية أهملت مساهمات الرنين في حسابات قيم معدلات التفاعل.

## 1- Introduction

Asymptotic Giant Branch (AGB) represents an important stage of stellar phases that supplement the universe with elements heavier than iron. The observation of heavy-element abundances on the surface of these stars, made by Merrill in 1952, provided conclusive evidence that nuclear activity involving a sequence of slow neutron capture process (*s-process)* is taking place in their interior, via which a series of stable isotopes is formed [1]. Later on, independent, extensive studies of Caughlan, Fowler and Iben & Renzini, along with numerical modeling of AGB stellar nucleosynthesis by Gallino *et al*. They all confirmed that two neutron donor reactions mainly supply the *s-process* with the necessary neutron fluxes in this type of stars, $^{13}C(\alpha, n)^{16}O$ and $^{22}Ne(\alpha,n)^{25}Mg$, with a major and minor contributions from the former and the latter reaction, respectively [2]. However, despite their low Gamow windows, their influence in elements synthesis up to $^{209}Bi$, in addition to their contribution in the production of about half of the heavy nuclei of the universe, made the $^{13}C(\alpha, n)^{16}O$ and $^{22}Ne(\alpha,n)^{25}Mg$ reactions attract great attention in many astrophysical studies [2- 5]. Thus, in this work, the thermonuclear reaction rates of these reactions will be studied, through investigating the impact of the spherical optical model potential on the cross-section calculations based on the Hauser-Feshbach (HF) model, and accordingly, the S-factor. The modeling of selected reactions used EMPIRE 3.2.2 Malta nuclear reaction model code [6] with two spherical optical models parameter sets from MFS [7], and AH [8]. These were used for determining the $T_c$ parameter, the Modified Lorentzian model for gamma strength function, width fluctuation correction based on Hofmann, Richert, Tepel, and Weidenmuller (HRTW) model, and Gilbert-Cameron model for level density calculations. Input parameters were executed from the *Reference Input Parameters Library* (RIPL-3) database.

## 2. Neutrons Source from AGB Stars

During the AGB phase of low-and-intermediate mass stars, the stellar structure is characterized by two distinct regions: The outer region which encloses the star by a large convective envelope and the inner region made by carbon/oxygen degenerate core. The main-component of the *s-process* synthesis begins its path. This component is usually activated as soon as neutrons seed is provided through two key reactions: $^{13}C(\alpha,n)^{16}O$ and $^{22}Ne(\alpha,n)^{25}Mg$.

These reactions are considered as the main neutron's sources in AGB stars. They frequently occur in a thin He-rich region with a solar mass ($M_\odot$) of $10^{-2} - 10^{-3}$ between the He and H shells, called the "intershell" region [9]. Under specific conditions, one of these reactions will dominate over the other. For instance, $^{13}C(\alpha,n)^{16}O$ reaction controls neutron production during the early phase of AGB stars with a mass of $1.5 - 4\ M_\odot$, in which the dominant energy source is the H-shell, with small periodic contributions from the He shell. The occurrence of this reaction depends essentially on the presence of the $^{13}C$ isotope, which is regularly created during a mixing episode ("dredge-up") between the envelope and the intershell region [10]. As a consequence of this dredge up process, a rich $^{13}C$ pocket

will be created via $^{12}C(p,\gamma)\,^{13}C$ reaction, providing the raw material for the $^{13}C(\alpha,n)^{16}O$ reaction to take place. However, once the intershell temperature reaches around $9\times10^7$ K, the $\alpha$- particles attain sufficient energies to initiate the $^{13}C(\alpha,n)^{16}O$ reaction. Subsequently, a thin layer with rich neutron density ($\sim 10^8 cm^{-3}$) is created, commencing the main-component of the *s-process* for about $10^4$yr [11].

For more massive $(4-8)M_\odot$ AGB stars, $^{22}Ne(\alpha,n)^{25}Mg$ reaction will be dominating as the main neutron source. This reaction is usually activated during thermal pulses in the intershell region as the temperature exceeds $\sim 3\times10^8$K [12], producing a substantial amount of neutrons. Even though this reaction has a short timescale (order of years), its contribution plays a significant role in the enhancement of the neutron density profiles up to $10^{13}cm^{-3}$ [13], which in turn opens many branching points in the main-component under these conditions. Moreover, besides its considerable contribution to the main component, the $^{22}Ne(\alpha,n)^{25}Mg$ reaction is also considered as the ruling neutron source of the weak *s-process* component, which frequently operates at the end of the He burning and/ or during the convective carbon-shell burning of massive stars ($> 8\,M_\odot$). This provides the star with an appreciable flux of neutrons that is contributing to the production process of all isotopes between iron and yttrium [14].

Hence, it is of importance to characterize these two key reactions by means of reaction rates and over a wide range of energy relevant to a stellar temperature of the order of $(10^7-10^9)$ K, starting from the threshold of Coulomb barrier of up to a few MeV's. In particular, α reaction cross-section goes through some regions with definitive resonance peak (or peaks) alongside the smoothly-varying nonresonant regions.

**3. Thermonuclear Reaction Rates**

For two reactant particles at a given temperature T, the Maxwellian-averaged reaction rate per particle pair $\langle\sigma v\rangle$ is [15],

$$\langle\sigma v\rangle = \left(\frac{8}{\pi\mu}\right)^{\frac{1}{2}}(k_BT)^{-3/2}\int_0^\infty E\,\sigma(E)e^{-E/kT}dE \qquad \ldots..(1)$$

where $\mu$ is the reduced mass $\mu=\frac{m_0m_1}{m_0+m_1}$ of interacting particles 0 and 1, $k_B$ is Boltzmann constant, $E$ is the incident energy in center-of-mass frame, and $\sigma(E)$ is the reaction cross section at a given $E$.

From Eq. (1), it is seen that the backbone of determining stellar reaction rates is the cross-section, which in most cases has a cumulative contribution from both nonresonant and resonant components. In this study, we will focus on the nonresonant contribution, as it governs the rate of thermonuclear reactions over a wide energy range.

Due to their low cross-sections and low tunneling probabilities, the measurements of stellar reactions in a laboratory under stellar conditions represent a very difficult task and, in some cases, it is even impossible to obtain. Therefore, a less energy-dependent factor is introduced in the astrophysical calculations rather than the cross-section that is the S-factor. The astrophysical S-factor, $S(E)$, is typically a smooth, slow-varying function of energy that gives the probability of a reaction to take place. For a charged-particle induced reaction [16],

$$S(E)=\sigma(E)Ee^{2\pi\eta(E)} \qquad \ldots\ldots\ldots..(2)$$

where $\eta(E)$ is the Sommerfeld parameter,

$$\eta(E)=\ 0.1575\,Z_0Z_1\left(\frac{\mu}{E}\right)^{\frac{1}{2}} \qquad \ldots..(3)$$

and $Z_0, Z_1$ are the projectile and target atomic numbers, respectively. In most cases, it is more convenient to describe the experimental or theoretical S-factor as the first three terms of a Taylor series around zero $E$ but far from nuclear resonance,

$$S(E)\approx S(0)+\dot{S}(0)E+\frac{1}{2}\ddot{S}(0)E^2 \qquad \ldots.(4)$$

where the dot indicates differentiation with respect to energy. Substituting this expansion and Eq. (2) in Eq. (1) yields [17],

$$N_A\langle\sigma v\rangle=\frac{4.339\times10^8}{Z_0Z_1}\frac{M_0+M_1}{M_0M_1}S_{eff}e^{-\tau}\,\tau^2..(5)$$

with $N_A$ is the Avogadro's number and

$$S_{eff} = S(0)\left[1 + \frac{5}{12\tau} + \frac{\dot{S}(0)}{S(0)}\left(E_0 + \frac{35}{36}kT\right) + \frac{1}{2}\frac{\ddot{S}(0)}{S(0)}\left(E_0^2 + \frac{89}{36}E_0 kT\right)\right] \ (MeV.b) \quad ..(6)$$

$$E_0 = 0.122\left(Z_0^2 Z_1^2 \frac{M_0 M_1}{M_0 + M_1} T_9^2\right)^{1/3} \ (MeV) \quad ..(7)$$

$$\tau = \frac{3E_0}{kT} = 4.2487(Z_0^2 Z_1^2 \mu / T_9)^{1/3} \quad \ldots\ldots\ldots\ldots..(8)$$

Due to their fundamental importance in determining the reaction rates for many astrophysical applications, especially at energies below the Coulomb barrier, several statistical models such as Weisskopf-Ewing [18], Hauser-Feshbach [19] alongside quantum mechanical models [20,21] were established to compute the cross-section and, consequently, the S (E) through Eq. (2).

**4. Hauser-Feshbach Formula**

At stellar conditions where the excitation energies of the incident particles are frequently low (few keV to about 2 MeV), the nuclear reactions are dominated by compound nucleus (CN) reaction, in which the reaction mechanism is accomplished by the CN formation followed by its decay on a time scale of about $10^{-18}s$ or more [22]. However, according to Bohr's hypothesis, this decay process of the CN in a given exit channel depends basically on the ratio of its probability to decay in this specific channel with respect to all other possible channels. However, it does not depend on the formation mechanism of the CN. This approximation is formally translated into the Hauser-Feshbach equation, in which the decay probability function of the CN to a specific channel is given in terms of transmission coefficients [6],

$$\sigma_{a,b}^{HF}(E) = \sum_{J\pi} \sigma_a^{CN}(E, J\pi) \frac{T_b(E_x, J\pi)}{\sum_c T_c(E_x, J\pi)} \quad \ldots\ldots\ldots..(9)$$

where $\sigma_{a,b}^{HF}$ is the Hauser-Feshbach cross-section and $\sigma_a^{CN}(E, J\pi)$ is the compound nucleus formation cross-section in a state of spin and parity $J\pi$ associated to the incident channel $a$. $T_b(E_x, J\pi)$ is the transmission coefficient of the outgoing particle that can be a particle or a photon and $T_c$ is the transmission coefficient in channel $c$ calculated with the optical model $S$-matrix element $T_c = 1 - |\langle S_{cc}\rangle|^2$.

One of the most important facts of the Hauser-Feshbach theory is its consideration of both total angular momentum and parity conservation laws. Nevertheless, it misleads an essential fact, which is the correlations between the entrance and exit channels amplitudes. Thus, a correction factor known as a width fluctuation correction was entered to the original formula as [23],

$$\sigma_{a,b} = {\sigma_{a,b}}^{HF} W_{a,b} \quad \ldots\ldots\ldots..(10)$$

where $\sigma_{a,b}$ is the energy average cross-section from channel $a$ to $b$ and $W_{a,b}$ is the width-fluctuation correction factor.

Many implementations of HF theory were made before to improve the results of various physical parameters of Eqs. 8 and 9 with the aid of computer codes. In this work, only the influence of the optical model potential on the S-factor and non-resonant reaction rate per particle calculations were considered.

**5. Reaction Rate Enhancement Factor: Electron Screening**

The numerical formula for reaction rate, Eq. (1), is usually evaluated by assuming pure electrostatic interaction between two bare unscreened nuclei. However, in stellar interiors, where the temperature and density are considerable, the reactant nuclei are immersed in a spherically symmetric, negatively-charged cloud of free electrons that acts as a screening potential for projectile against the Coulomb repulsive barrier. This results in an effect similar to the one obtained from the atomic orbital electrons screening [24].

Due to this shielding, the incoming projectile experiences a reduction in the Coulomb barrier potential by an amount of $U_e$, which consequently increases the reaction cross section through modifying the penetration factor.

Commonly, the screened reactivity of a charged particle-induced reaction can exist as a product of the regular stellar reactivity $\langle\sigma v\rangle$ and the screening enhancement factor $f(E)$,

$$\langle\sigma v\rangle_{screened} = f(E)\,\langle\sigma v\rangle \quad \ldots\ldots..(11)$$

with

$$f(E) = \frac{\sigma_s(E)}{\sigma_b(E)} = \frac{\sigma_b(E+U_e)}{\sigma_b(E)} \approx \exp\left(\pi\eta(E)\frac{U_e}{E}\right) \quad \ldots\ldots\ldots\ldots\ldots (12)$$

where $\sigma_s$ and $\sigma_b$, respectively, stand for the screened and bare nuclei cross sections at the center-of-mass energy $E$, and $\eta$ is the Sommerfeld parameter.

## 6. Calculations and Discussion

### 6.1 Astrophysical Factor and Reaction Rate

Two spherical optical model parameter sets of MFS [7] and AH [8] were utilized for determining the cross section of the $^{13}C(\alpha,n)^{16}O$ and $^{22}Ne(\alpha,n)^{25}Mg$ reactions using EMPIRE nuclear code [6], and their results are shown in Fig. (1). The comparison of cross sections with EXFOR data showed a close similarity between the results of using MFS parameters and experimental data. But there is a quite high difference by about a factor of 3 at energy 0.5 MeV when using the parameters of AH. This discrepancy was resulted from the high value of diffuseness parameter of the real potential term for AH, which is $a \approx 0.797$ fm and $a \approx 0.793$ fm for $^{13}C$ and $^{22}Ne$, respectively [7], comparing to that for MFS which is $a \approx 0.55$ fm for both reactions [8]. Consequently, it caused an overestimation of the cross section value, especially at low energies region where the elastic scattering is predominantly sensitive to the tail region of the optical potential.

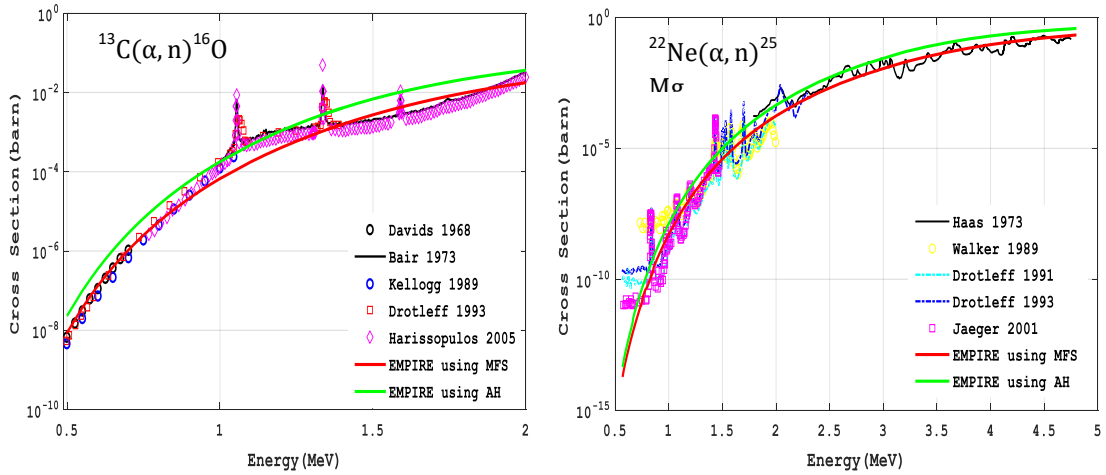


**(a** **(b**

**Figure (1):** Comparison of the cross-sections obtained using MFS and AH parameters set with measured data extracted from EXFOR for: (a) $^{13}C(\alpha,n)^{16}O$ and (b) $^{22}Ne(\alpha,n)^{25}Mg$ reactions.

As the energy is increased to about 2 MeV for $^{13}C(\alpha,n)^{16}O$ and about 5 MeV for $^{22}Ne(\alpha,n)^{25}Mg$, the difference factor decreases to about (2–1.77), since at these energies the elastic scattering becomes more sensitive to the nuclear interior rather than the potential tail region. This occurs due to the enhancement of penetration probability through the Coulomb barrier with increasing incident energy. Both results which are based on MFS and AH parameters were used to calculate the S-factor values through Eq. (2), with extrapolating the data downward to zero energy to estimate the S-factor coefficients, as displayed in Figure-2.

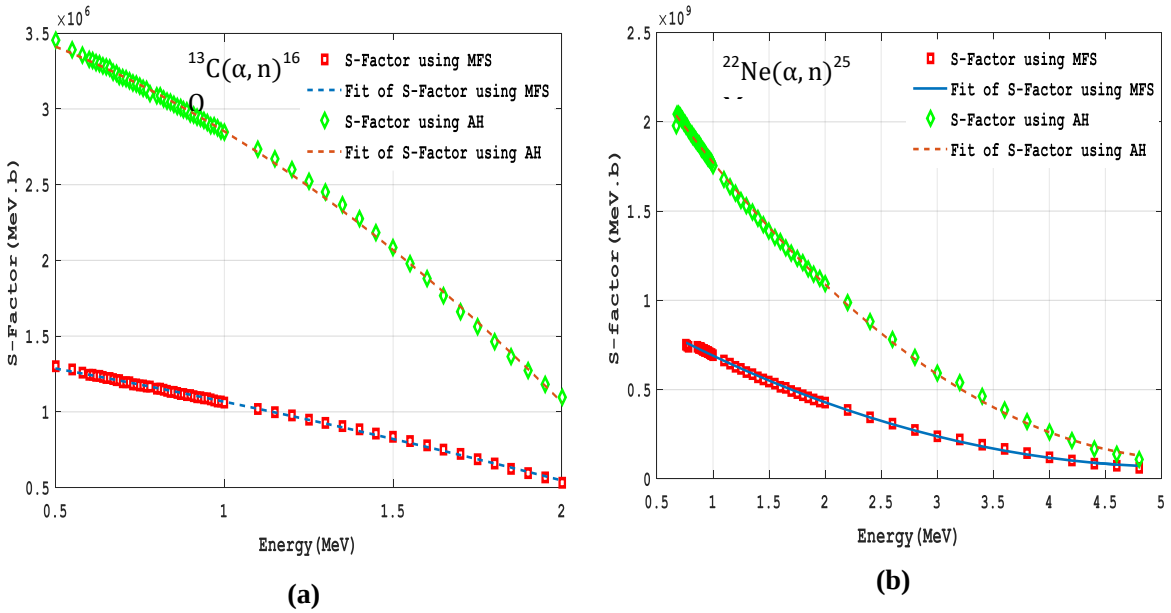


**Figure 2-** S-Factor fitting using EMPIRE calculated cross sections of both MFS and AH parameter sets for: (a) $^{13}C(\alpha,n)^{16}O$ and (b) $^{22}Ne(\alpha,n)^{25}Mg$ reactions.

**Table 1**-The resulted S(E) coefficients from fitting S(E) with respect to E for $^{13}C(\alpha,n)^{16}O$ and $^{22}Ne(\alpha,n)^{25}Mg$ reactions

| **Reaction** | **Adopted σ for calculating S(E)** | $S(0)$ **$10^6$ MeV. b** | $\dot{S}(0)$ **$10^6$ b** | $\ddot{S}(0)$ **$10^6$b. MeV$^{-1}$** |
|---|---|---|---|---|
| $^{13}C(\alpha,n)^{16}O$ | MFS | 1.48 | −0.35 | −0.1 |
| | AH | 3.7 | −0.44 | −0.89 |
| $^{22}Ne(\alpha,n)^{25}Mg$ | MFS | 1000 | −372 | 35 |
| | AH | 2600 | −950 | 90 |

From the extrapolation, an empirical polynomial formula for the total $S(E)$ equivalent to Eq. (4) was deduced, according to cross sections calculated using both MFS and AH sets and for the two reactions adopted in this work. The obtained coefficients of $S(E)$, $S(0)$, $\dot{S}(0)$, and $\ddot{S}(0)$ are listed in Table (1). For all cases, the coefficients of $S(E)$ values is included in Eq. (6) to estimate the reaction rate values through Eq. (5), and the numerical results are presented in Tables (2 and 3).

It was found, for $^{13}C(\alpha,n)^{16}O$ reaction, that the obtained $S(E)$ from MFS showed a good agreement with that of Johnson *et al.* [25], who reported a value of $1.2 \times 10^6$MeV. b at energy 0.1 MeV, and with NACREII [26] at energy 0.2 MeV that accounts $1.5^{+0.5}_{-0.4} \times 10^6$ MeV. b. Whereas the value resulted from using AH gave acceptable results in comparison with Heil *et al.* and Pellegriti *et al.*, with values of $3.3^{+1.8}_{-1.4} \times 10^6$ MeV. b and $3.4 \times 10^6$ MeV. b at energy 0.1 MeV, respectively, as found in their published results in La Cognata et al. [25]

On the other hand, for $^{22}Ne(\alpha,n)^{25}Mg$ reaction, the resulted value of $S(E)$ from the MFS-based cross section showed a good agreement with those based on NACRE [27] and BRUISLIB [26], with a value of about $0.8 \times 10^9$MeV. b at 0.2 MeV. While that attained by AH overestimated the $S(E)$ by a factor of about 3.25, in comparison to previously reported outcomes [27, 28].

**Table 2-** $^{13}C(\alpha, n)^{16}O$ unscreened $N_A\langle\sigma v\rangle$ and screened $EN_A\langle\sigma v\rangle$reaction rates in $cm^3\ mole^{-1}\ s^{-1}$ for temperatures of $0.01 \leq T_9 \leq 1$.

| $T_9$ | $N_A\langle\sigma v\rangle$ (MFS) | $EN_A\langle\sigma v\rangle$ (MFS) | $N_A\langle\sigma v\rangle$ (AH) | $EN_A\langle\sigma v\rangle$ (AH) |
|---|---|---|---|---|
| 0.01 | 2.60E-48 | 1.01E-46 | 6.53E-48 | 2.55E-46 |
| 0.02 | 4.55E-35 | 24.9E-35 | 1.15E-34 | 6.29E-34 |
| 0.03 | 1.20E-28 | 3.34E-28 | 3.03E-28 | 8.46E-28 |
| 0.04 | 1.33E-24 | 2.70E-24 | 3.38E-24 | 6.84E-24 |
| 0.05 | 1.00E-21 | 1.69E-21 | 2.55E-21 | 4.30E-21 |
| 0.06 | 1.57E-19 | 2.35E-19 | 3.98E-19 | 5.98E-19 |
| 0.07 | 8.82E-18 | 12.2E-18 | 2.24E-17 | 3.11E-17 |
| 0.08 | 2.44E-16 | 3.21E-16 | 6.24E-16 | 8.18E-16 |
| 0.09 | 4.05E-15 | 5.09E-15 | 1.03E-14 | 1.30E-14 |
| 0.1 | 4.54E-14 | 5.53E-14 | 1.16E-13 | 1.41E-13 |
| 0.12 | 2.43E-12 | 2.82E-12 | 6.22E-12 | 7.25E-12 |
| 0.14 | 5.80E-11 | 6.55E-11 | 1.49E-10 | 1.68E-10 |
| 0.16 | 7.93E-10 | 8.76E-10 | 2.04E-09 | 2.26E-09 |
| 0.18 | 7.22E-09 | 7.85E-09 | 1.87E-08 | 2.03E-08 |
| 0.2 | 4.82E-08 | 2.09E-08 | 1.25E-07 | 1.34E-07 |
| 0.25 | 2.16E-06 | 2.27E-06 | 5.62E-06 | 5.92E-06 |
| 0.3 | 3.88E-05 | 4.04E-05 | 1.01E-04 | 1.06E-04 |
| 0.35 | 3.88E-04 | 4.01E-04 | 1.02E-03 | 1.10E-03 |
| 0.4 | 2.50E-03 | 2.70E-03 | 6.83E-03 | 7.00E-03 |
| 0.5 | 5.00E-02 | 5.14E-02 | 1.34E-01 | 1.37E-01 |
| 0.6 | 4.80E-01 | 4.88E-01 | 1.29E+00 | 1.31E+00 |
| 0.7 | 2.89E+00 | 2.92 E+00 | 7.79E+00 | 7.88E+00 |
| 0.8 | 1.26E+01 | 1.27E+01 | 3.41E+01 | 3.45E+01 |
| 0.9 | 4.34E+01 | 4.37E+01 | 1.18E+02 | 1.19E+02 |
| 1 | 1.25 E+02 | 1.26E+02 | 3.43E+02 | 3.45E+02 |

**Table 3-** $^{22}Ne(\alpha, n)^{25}Mg$ unscreened $N_A\langle\sigma v\rangle$ and screened $EN_A\langle\sigma v\rangle$ reaction rates in $cm^3\ mole^{-1}\ s^{-1}$ for temperatures of $0.01 \leq T_9 \leq 1$.

| $T_9$ | $N_A\langle\sigma v\rangle$ (MFS) | $EN_A\langle\sigma v\rangle$ (MFS) | $N_A\langle\sigma v\rangle$ (AH) | $EN_A\langle\sigma v\rangle$ (AH) |
|---|---|---|---|---|
| 0.01 | 5.16E-75 | 1.83E-70 | 1.34E-74 | 4.75E-70 |
| 0.02 | 1.14E-55 | 1.48E-53 | 2.96E-55 | 3.84E-53 |
| 0.03 | 2.76E-46 | 5.22E-45 | 7.19E-46 | 136E-46 |
| 0.04 | 2.30E-40 | 1.72E-39 | 5.98E-40 | 44.9E-40 |
| 0.05 | 3.73E-36 | 16.6E-36 | 9.71E-36 | 43.2E-36 |
| 0.06 | 6.06E-33 | 19.3E-33 | 1.58E-32 | 5.04E-32 |
| 0.07 | 2.22E-30 | 5.66E-30 | 5.77E-30 | 14.7E-30 |
| 0.08 | 2.88E-28 | 6.27E-28 | 7.51E-28 | 16.3E-28 |
| 0.09 | 1.76E-26 | 3.4E-26 | 4.59E-26 | 8.86E-26 |
| 0.1 | 6.09E-25 | 10.7E-25 | 1.59E-24 | 2.79E-24 |
| 0.12 | 2.08E-22 | 3.22E-22 | 5.43E-22 | 8.39E-22 |
| 0.14 | 2.19E-20 | 3.1E-20 | 5.71E-20 | 8.09E-20 |
| 0.16 | 1.02E-18 | 1.35E-18 | 2.65E-18 | 3.53E-18 |
| 0.18 | 2.60E-17 | 3.31E-17 | 6.78E-17 | 8.63E-17 |
| 0.2 | 4.23E-16 | 5.2E-16 | 1.10E-15 | 1.36E-15 |
| 0.25 | 1.12E-13 | 1.3E-13 | 2.93E-13 | 3.40E-13 |
| 0.3 | 7.83E-12 | 8.78E-12 | 2.05E-11 | 2.29E-11 |
| 0.4 | 3.73E-09 | 4.02E-09 | 9.77E-09 | 10.5E-09 |

| | | | | |
|---|---|---|---|---|
| 0.5 | 2.94E-07 | 3.1E-07 | 7.70E-07 | 8.12E-07 |
| 0.6 | 8.05E-06 | 8.39E-06 | 2.12E-05 | 2.20E-05 |
| 0.7 | 1.12E-04 | 1.154E-04 | 2.94E-04 | 3.04E-04 |
| 0.8 | 9.66E-04 | 9.921E-04 | 2.54E-03 | 2.61E-03 |
| 0.9 | 5.91E-03 | 6.04E-03 | 1.56E-03 | 15.96E-03 |
| 1 | 2.78E-02 | 2.83E-02 | 7.40E-02 | 7.51E-02 |

**6.2 Screening Effect and Effective S-Factor**

The effect of electron shielding process was introduced in the reaction rate calculation as an enhancement factor $f(E)$, Eq. (12), and by using the analytical formulas of Liolios for $U_e$ [24],

$$U_e = -20.93 \times 10^{-6}\left[(Z_0 + Z_1)^{\frac{7}{3}} - Z_0^{\frac{7}{3}} - Z_1^{\frac{7}{3}}\right] MeV$$

which is established based on the Thomas-Fermi model and for Adiabatic Limit (AL) approximation, which is the most convenient approximation for the astrophysical reactions condition.

The resulted rate of the two reactions, adopted in this work after enhancement, are listed in Tables (2 and 3) and shown in Figs. 3 and 4. The figures illustrate that, at low temperature $T_9 < 0.1$ region, the shielding effect has a significant influence on the reaction rate value of both reactions, especially for targets with higher atomic number - in this case, $^{22}$Ne. This occurs because, at these temperatures, the response of electrons to the nuclear motion is nearly instantaneous and, hence, they can occupy the energetically most favorable configuration during collision. This substantially enhanced the reaction rate compared to the previous compilations where this effect was not considered, such as in the studies of Heil *et al.* [16], NACREII [26], Caughlan and Fowler [29], NACRE [27], and BRUISLIB [28], as displayed in Figs. (4 and 5).

However, as the temperature increases, $T_9 \geq 0.1$, the projectile energy raises, and it passes through the target with a fast velocity that the electrons cannot provide the necessary shielding for it against the repulsive Coulomb potential. Consequently, the effective screening potential becomes nearly constant, and it will have a small influence on the reaction rate, as shown in Figure-3.

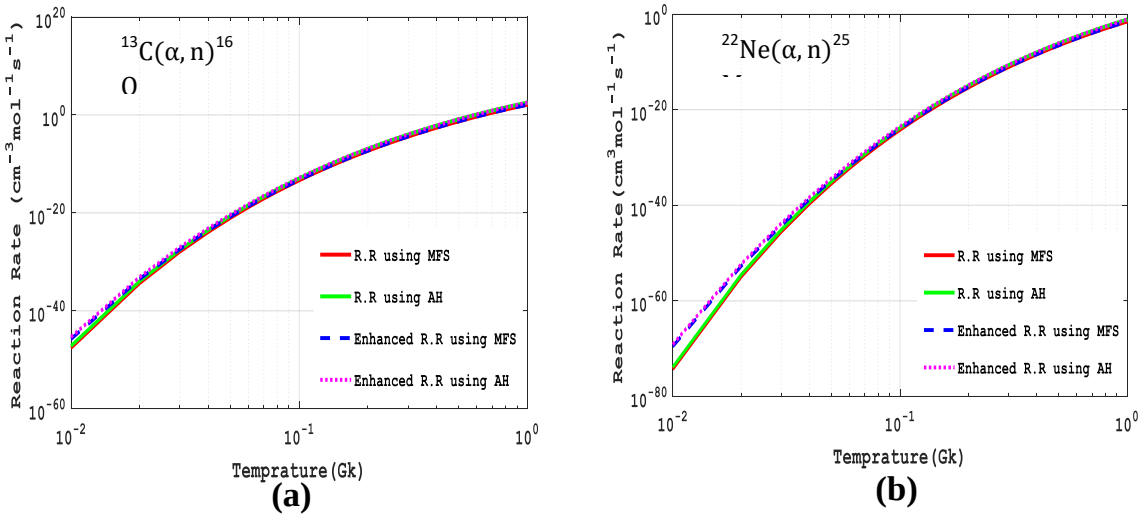


**Figure (3):** The enhanced reaction rate resulted from using AL approximation in comparison with uncorrected result obtained for: (a) $^{13}$C(α, n)$^{16}$O and (b) $^{22}$Ne(α, n)$^{25}$Mg reactions from using both MFS and AH.

Moreover, the comparison in Figs. (4 and 5) clearly demonstrates that, even though the shielding effect provides little enhancement for the reaction rate values at a temperature of $T_9 \geq 0.1$, but our results are still higher than those obtained from previously mentioned compilations. This is owing to the use of $S_{eff}$ value in our calculations, in contrary to the reports of other authors [16, 26-28], who applied $S(E)$. This factor was found to have a major effect on modifying the rate in the low-temperature region, as it takes into account the fact that the area under the curve of the Gamow peak is

not equal to that of a Gaussian, although it has an approximately Gaussian's shape with a similar maximum at $E = E_0$.

Furthermore, for both adopted reactions, the ratio of our rates to those of Caughlan and Fowler [29] showed a rapid decline at $T_9 > 0.04$, even though both our and their studies used the $S_{eff}$ rather than $S(E)$ value. This fact can be explained by the fact that, according to Caughlan and Fowler's calculations, their estimate of the reaction rate was based on the value of $S_{eff}$, which was resulted from Fowler et al. [30] who ignored the coefficients $\dot{S}(0)$ and $\ddot{S}(0)$ terms in their calculations. That, in turn, caused an overrating of their rate values, especially in the high energy regions.

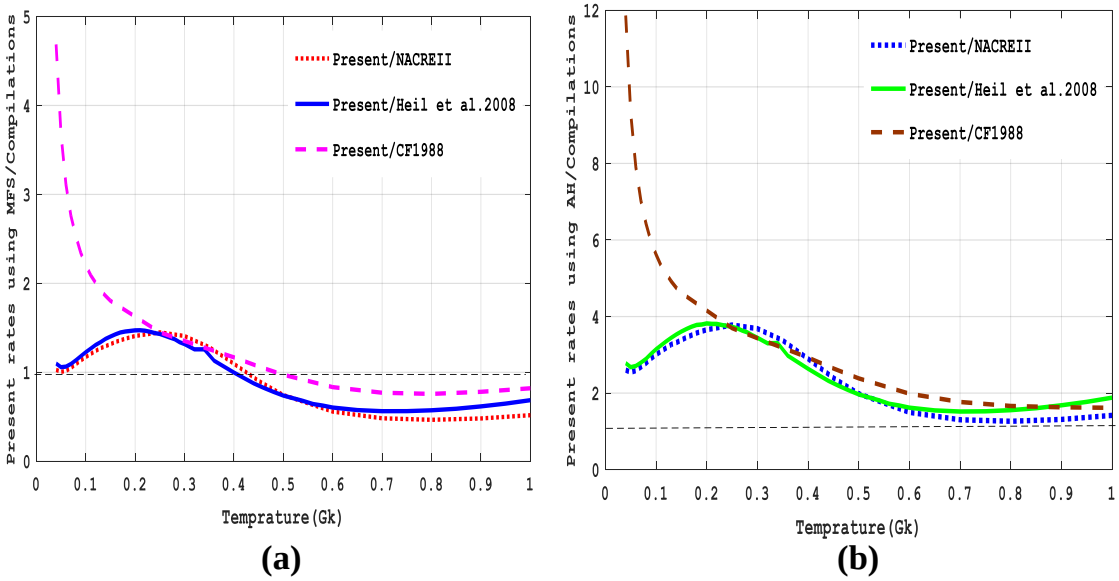


**Figure 4**-Present rates reaction of $^{13}C(\alpha, n)^{16}O$ in comparison to NACREII, Heil et al. and the CF rates for temperatures of $0.01 \leq T_9 \leq 1$, obtained using (a) MFS, (b) AH.

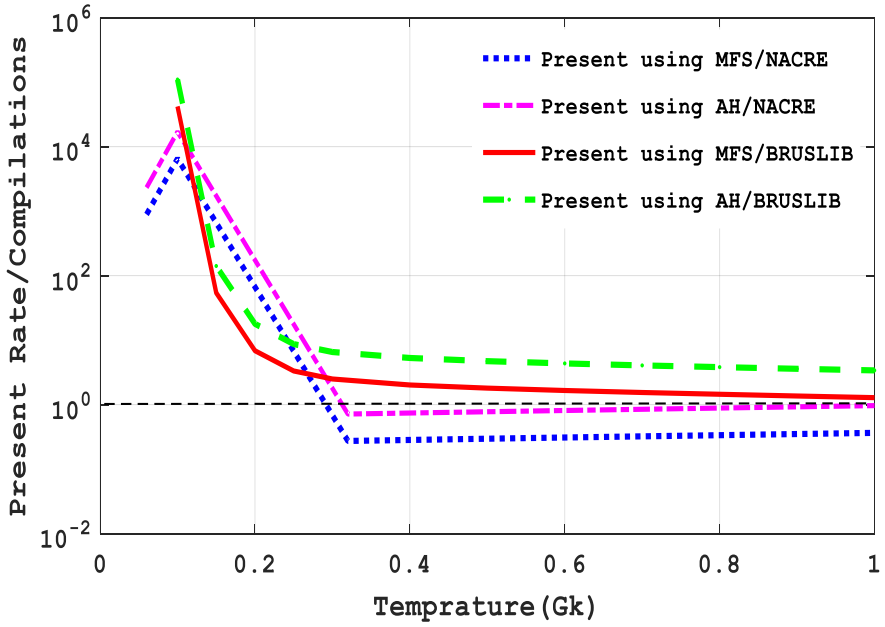


**Figure 5**- Present rates of $^{22}Ne(\alpha, n)^{25}Mg$ reaction in comparison to the NACRE and BRUSLIB rates for temperatures of $0.09 \leq T_9 \leq 1$, obtained using MFS, and AH.

On the other hand, for a temperature above $T_9 = 0.2$, the current rates of $^{13}C(\alpha,n)^{16}O$ reaction begin to show a shallow decrease with increasing temperature in comparison to other compilations and for each of the resulting values of $S(E)$, as displays in Fig. (4). This is because, at these temperatures, the $^{13}C(\alpha,n)^{16}O$ is dominated by the production through the tail of the $1/2^+$ resonance state in $^{17}O$, located at $E_r = 6356$ keV. That was not taken into account in this study, in contrary to other previous studies [16, 27, 29]. The same fact was also noticed in our results of $^{22}Ne(\alpha,n)^{25}Mg$ reaction at the relevant temperatures region of $T_9 > 0.1$, but with much higher impact. This occurred due to the fact that, at these temperatures, the rate is vastly dominated by two resonance contributions in the $^{26}Mg$ compound nucleus at $E_r = 633$ keV and $E_r = 828$ keV, which was also not included in this study, in comparison to earlier works [27, 28].

**7. Conclusions**

The calculated reaction rates through HF model were shown to be highly dependent on the optical model potential variations. It was shown that a difference of about $\approx 0.24$ fm in the diffuseness parameter for the real potential term between MFS and AH parameters sets, caused an overestimate of the $S(E)$ value by about a factor of 2.43 and 2.6 for both $^{13}C(\alpha,n)^{16}O$ and $^{22}Ne(\alpha,n)^{25}Mg$ reactions, respectively. This consequently exaggerated the obtained rates from the value of S-factor calculated from AH in comparison to that from MFS. Moreover, for both adopted reactions, the reaction rates obtained using $S(E)$ values results from MFS displayed a good agreement with previous compilations, with a low variation of about $\pm 0.5$ for $^{13}C(\alpha,n)^{16}O$ reaction and a higher discrepancy of about $1.5^{+0.2}_{-2.3}$, for $^{22}Ne(\alpha,n)^{25}Mg$, at a temperature above 0.3 GK. These disparities are owing to the significant influence of resonance contributions on these reactions, especially on $^{22}Ne(\alpha,n)^{25}Mg$, which was ignored in this work. However, although the resonance contribution is currently skipped, the values of reaction rates based on $S(E)$ computed according to AH set were found to exceed all the results obtained by forgoing stated compilations and overall temperature range adopted, as shown in Figs. (5,6), which is a reflection of the overestimation of $S(E)$ values resulted from AH. On the other hand, for temperatures below 0.1 GK, in which $^{13}C(\alpha,n)^{16}O$ reaction is activated, the shielding process was found to have a crucial role in enhancing the reaction rate values of both reactions, and with a more relative impact on $^{22}Ne(\alpha,n)^{25}Mg$ reaction.

**References**


1. Burbidge, E., *et al.*, **1957**. Synthesis of the elements in stars. *Reviews of modern physics*, **29**: 548-650.
2. Liu, N., *et al.*, **2018**. New Constraints on the major neutron source in low-mass AGB Stars. *The astrophysical journal*, **865**:112-126.
3. Gallino, R., **1998**. Evolution and nucleosynthesis in low-mass asymptotic giant branch stars. II. Neutron capture and the s-process. *The astrophysical journal*, **497**: 388-403.
4. Trippella, O. and La Cognata, M., **2017**. Concurrent application of ANC and THM to assess the $^{13}C(\alpha, n)^{16}O$ absolute cross section at astrophysical energies and possible consequences for neutron production in low-mass AGB stars. *The astrophysical journal*, **837**:41-53.
5. Jayatissa, H., **2020**. Constraining the $^{22}Ne(\alpha,\gamma)^{26}Mg$ and $^{22}Ne(\alpha,n)^{25}Mg$ reaction rates using sub-Coulomb α-transfer reactions. *Physics Letters B*, **802**: 1-6.
6. Herman, M., *et al.*, **2007**. EMPIRE: Nuclear Reaction Model Code System for Data Evaluation, *Nuclear data sheets*, **108**: 2655-2715.
7. McFadden L. and Satchler G., **1966**. Optical-model analysis of the scattering of 24.7 MeV alpha particles. *Nuclear physics*, **84**: 177-200.
8. Avrigeanu V. and Hodgson P. E., **1996**. Global optical potentials for emitted alpha particles. *Physical review*, **49**: 2136-2141.
9. Lugaro M., et al., **2003**. *s-process* nucleosynthesis in asymptotic giant branch stars: A test for stellar evolution. *The astrophysical journal*, **586**: 1305–1319.
10. Pignatari M., et al., **2005**. Effect of uncertainty of the $^{13}C(\alpha,n)^{16}O$ and $^{22}Ne(\alpha,n)^{25}Mg$ reaction rates in the *s-process*. *Nuclear physics A*, **758**: 541c–544c.
11. Cristallo S., et al., **2018**. The importance of the $^{13}C(\alpha,n)^{16}O$ reaction in asymptotic giant branch stars. *The astrophysical journal*, **859**: 105-119.

**12.** Tain J. L., et al., **2016**. Measurement of very low $(\alpha, n)$ cross sections of astrophysical interest. *Journal of physics*: Conf. Ser. **665**: 012031.
**13.** Lugaro M., **2016**. Neutron sources and neutron-capture paths in asymptotic giant branch stars". *Journal of Physic*.: Conf. Ser. **703:** 012003.
**14.** Talwar R., **2015**. *Stellar neutron sources and s-process in massive stars*. PhD. diss, University of Notre Dame, USA.
**15.** Gallino R., et al., **1998**. Evolution and nucleosynthesis in low-mass asymptotic giant branch stars II. Neutron capture and *s-process.* The *astrophysical journal*, **497**: 388.
**16.** Heil M., et al., **2008**. The $^{13}C(\alpha, n)$ reaction and its role as a neutron source for the *s*-process. *Physical review C*, **78**: 025803.
**17.** Iliadis C., **2015**. *Nuclear Physics of Stars*. 2nd ed. Weinheim. Wiley-VCH Verlag GmbH & Co. KGaA, Germany.
**18.** Weisskopf V. and Ewing D., **1940**. On the Yield of Nuclear Reactions with Heavy Elements. *Physical review*, **57**: 472–485.
**19.** Hauser W. and Feshbach H.,**1952**. The Inelastic Scattering of Neutrons. *Physical review*, **87**: 366–373.
**20.** Kapur P. L. and Peierls R. E., **1938**. The dispersion formula for nuclear reactions. *The royal society A*, **166**: 277- 295.
**21.** Balantekin A.,**1998**. Quantum Tunneling in Nuclear Fusion. *Nuclear theory*,**70**: 77-100.
**22.** Betak E. and Hodgson P. E., **1998**. Particle–hole state densities in pre-equilibrium nuclear reaction models. Report program of physics, **61**: 483.
**23.** Kawano T., **2015**. Challenges beyond Hauser-Feshbach for nuclear reaction modeling. *The European physical journal A*, **51**: 164- 171.
**24.** Liolios T., **2001**. Atomic effects in astrophysical nuclear reactions. *Physical review C*, **63**: 045801.
**25.** La Cognata M., et al., **2013**. On the measurement of the $^{13}C(\alpha, n)^{16}O$ S-Factor at negative energies and its influence on the *s-process*. *The astrophysical journal*, **777**:143.
**26.** Xu Y., et al., **2013**. NACREII: An update of the NACRE compilation of charged-particle-induced thermonuclear reaction rates for nuclei with mass number A<16. *Nuclear physics*, **918**: 61–169.
**27.** Angulo C., et al., **1999**. A compilation of charged-particle induced thermonuclear reaction rates. *Nuclear physics A*, **656**: 3-183.
**28.** Xu Y., et al., **2013**. Databases and tools for nuclear astrophysics applications. *Astronomy and astrophysics*, **549**: A106.
**29.** Caughlan G. and Fowler W., **1988**. Thermonuclear reaction rates V*. *Atomic data and nuclear data tables*, **40**: 283-334.
**30.** Fowler W. et al., **1975**. Thermonuclear reaction rates. *Annual review of astronomy and astrophysics*, **13**: 69-112.